Compact lidar system using laser diode, binary continuous wave power modulation, and an avalanche photodiode-based receiver controlled by a digital signal processor

Antoni Ardanuy
Adolfo Comerón

Compact lidar system using laser diode, binary continuous wave power modulation, and an avalanche photodiode-based receiver controlled by a digital signal processor

Antoni Ardanuy and Adolfo Comerón*
Universitat Politècnica de Catalunya, CommSensLab, Department of Signal Theory and Communications, Barcelona, Spain

Abstract. We analyze the practical limits of a lidar system based on the use of a laser diode, random binary continuous wave power modulation, and an avalanche photodiode (APD)-based photoreceiver, combined with the control and computing power of the digital signal processors (DSP) currently available. The target is to design a compact portable lidar system made all in semiconductor technology, with a low-power demand and an easy configuration of the system, allowing change in some of its features through software. Unlike many prior works, we emphasize the use of APDs instead of photomultiplier tubes to detect the return signal and the application of the system to measure not only hard targets, but also medium-range aerosols and clouds. We have developed an experimental prototype to evaluate the behavior of the system under different environmental conditions. Experimental results provided by the prototype are presented and discussed. © *The Authors. Published by SPIE under a Creative Commons Attribution 3.0 Unported License. Distribution or reproduction of this work in whole or in part requires full attribution of the original publication, including its DOI.* [DOI: 10.1117/1.OE.57.4.044104]

1 Introduction

The application of lidar systems began with the use of high peak-power lasers. Even today most of the lidar systems in use for atmospheric remote sensing are based on this principle. A pulse of light of high peak-power is emitted from a laser, backscattered by atmospheric particulates and molecules, and collected by a telescope, and the return optical power is converted to an electrical signal by a photodetector. The use of high peak-power lasers entails two disadvantages, namely the necessary power to operate them and the lack of eye safety.

To overcome these problems, lasers with low peak-power and high pulse-repetition frequencies, in the tens of kHz, along with pulse-return accumulation can be used.[1] More efficient methods using continuous-wave (CW) low peak-power lasers power-modulated with sequences with properties similar to those of the sequences used in spread-spectrum communication systems[2,3] have been studied.[4–6] Detection using a correlation algorithm provides range resolution.

Many of the systems described until now using CW laser-diode transmitters employ photomultiplier tubes in the receiver system. However, the fast increase in the performance of digital signal processors (DSP) permits the envisioning of the use of long coding sequences with short processing times—a 200-point correlation using a sequence of 2047 bits takes a maximum time of 400 ms approximately—making practical a low-power consumption, eye-safe, and compact-size all-semiconductor lidar system, with laser-diode

transmitters and avalanche photodiodes (APDs) in the receiver system. The system can detect from low to high clouds, but it can be used in the detection of medium-range aerosol (see Sec. 6). A limitation in these systems arises from the condition to constrain the laser peak power to a maximum value that leads to a reduction in the signal-to-noise ratio (SNR) when the spatial resolution is increased if the laser peak power is kept constant (see Sec. 3). The low-energy consumption makes these systems attractive from the portability point of view. For example, the maximum power necessary for the system presented in this paper is below 10 W considering all the electronic and optoelectronic components. The telescope size would set the final limit to this portability.

The use of a DSP permits the implementation of an all-programmable system, with the possibility of changing the algorithms to detect the signals and the use of long sequences to extract the signal from the noise. A programmable system can adapt its performance to the needs of each moment or each application. Additionally, the use of DSPs allows the synchronization and total control of the transmitted and received signals, which is very important to avoid the degradation of the SNR.

The paper is organized as follows: Sec. 2 lays out the model of a system using pseudorandom sequences to modulate the power of a laser diode transmitter under the control of a DSP that is also in charge of performing the correlation operations to retrieve the range-resolved atmospheric backscatter. Section 3 presents the SNR gain of the system and the SNR at the output. Section 4 discusses the basic constraints of the system and the relation between the laser power, the electrical bandwidth, and the SNR. Section 5 shows the

*Address all correspondence to: Adolfo Comerón, E-mail: comeron@tsc.upc.edu

effect of nonlinearities and offsets in the system, which to our knowledge has not been dealt with in previous related literature, and finally Sec. 6 shows experimental results from the implemented prototype. Section 7 presents conclusions and gives an outlook of possible developments using the discussed lidar architecture.

2 System Modeling

The outline of a lidar system, independently of the used technology, is well known. Classically, single pulses are processed. The pulses can be either of high energy at a low repetition frequency or of low energy at a high repetition rate. Accumulating the returned pulses is equivalent to a processing gain. In the case of random binary CW modulation, the processing gain is obtained from the cross correlation of the received sequence with a reference sequence. In this way, the duty cycle, tending to 50%, is higher than in the other lidar systems, and the peak power can be reduced.

The received power from a range z in a pulsed lidar is given by the lidar equation[7]

$$P_{\text{received}}(z) = P_0 A_T \frac{c\tau}{2z^2} \beta(z) \exp\left[-2\int_0^z \alpha(x)\mathrm{d}x\right], \quad (1)$$

where P_0 is the transmitted laser-pulse power, A_T is the telescope effective area, c is the speed of light, τ is the pulse duration, z is the distance to the scattering atmosphere resolution cell, β is the atmospheric backscatter coefficient (units $\mathrm{m}^{-1}\,\mathrm{sr}^{-1}$), and α is the atmospheric extinction coefficient (units m^{-1}), which is integrated along all the two-way path to the target at distance z. Geometrical overlap effects have been disregarded.

For a CW pseudorandom sequence-modulated lidar (or CW-PRN lidar), it is convenient to cast the lidar equation as

$$
\begin{aligned}
&P_{\text{received}}(t)\\
&= P_0 A_T \int_0^\infty s\left(t - \frac{2z}{c}\right) \frac{\beta(z)}{z^2} \exp\left[-2\int_0^z \alpha(x)\mathrm{d}x\right]\mathrm{d}z,
\end{aligned}
$$
$$(2)$$

where P_0 is the maximum laser power and $s(t)$ is the power-modulating signal. In our case, $s(t)$ is a discrete pseudorandom sequence. Note that the integral in the right member of Eq. (2) is essentially a convolution of the sequence $s(t)$ with a function $h(z) = \frac{\beta(z)}{z^2} \exp[-2\int_0^z \alpha(x)\mathrm{d}x]$ that depends on the state of the atmosphere. We are interested in retrieving the

attenuated backscatter $\beta(z)\exp[-2\int_0^z \alpha(x)\mathrm{d}x] = z^2 h(z)$ or at least something proportional to it, i.e., the in general so-called range-corrected signal.

To evaluate the performance of the proposed CW lidar, we use the model of Fig. 1, where the input (the transmitted sequence) is known and the impulse response $h(z)$ is the function to evaluate. In this context, anticipating the digital signal processing to be carried out on the signal, the time functions are expressed as sample sequences, and, from now on, a discrete system will be assumed. According to Fig. 1, $s(n)$ is the transmitted sequence that yields an output $x(n)$ after passing through the channel with impulse response $h(n)$. The channel also adds a background radiation that contributes a noise $b(n)$. The received signal is pre-processed by the optoelectronic receiver, physically consisting of a telescope with effective collecting area A_T, an APD-based photoreceiver with voltage responsivity R_V, and an amplifier with gain g. Inevitably, the receiver also adds some noise represented by $w(n)$ at the input of the amplifier. The receiver output is sampled and digitized by the analogue-to-digital (A/D) converter, after which the processor produces an estimate of $h(n)$ based on the knowledge of $s(n)$.

After Fig. 1, the signal reaching the receiver is

$$y(n) = P_0 s(n) * h(n) + b(n) + c_s, \quad (3)$$

where $s(n)$ is the sequence modulating the transmitted power, $h(n)$ is the discrete impulse response of the channel (the atmosphere in this case), the symbol $*$ denotes the convolution operation, $b(n)$ is the shot noise added by the channel because of the detection of background radiation, and c_s is the offset value associated to the background radiation.

The discretized impulse response $h(n)$ can be written from Eq. (2) as

$$h(n) = \frac{c\tau_{\text{bit}}}{2} \frac{\beta\left(\frac{cn\tau_{\text{bit}}}{2}\right)}{\left(\frac{cn\tau_{\text{bit}}}{2}\right)^2} e^{-2\int_0^{\frac{cn\tau_{\text{bit}}}{2}} \alpha(x)\mathrm{d}x}, \quad (4)$$

where τ_{bit} is the duration of a bit in the sequence $s(n)$.

The output of the photoreceiver is

$$y_D = \{A_T R_V P_0[s(n) * h(n) + b(n) + w(n)] + c_{sr}\}g, \quad (5)$$

where A_T is the telescope effective collecting area, R_v is the photodetector responsivity, g is the gain of an amplifier chain accommodating the output amplitude of the photodetector to the input of the A/D converter (accommodation gain), $w(n)$
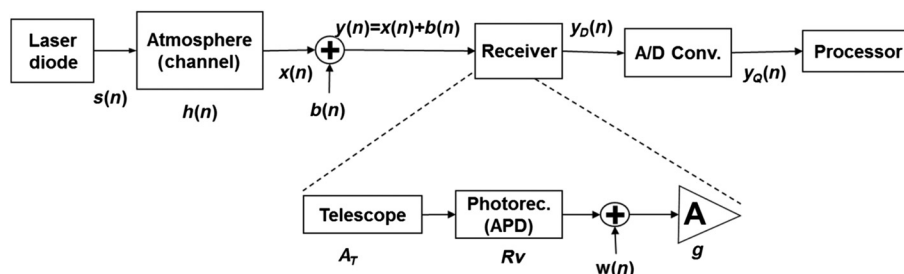

Fig. 1 Equivalent block chain of the lidar system.

is the noise added by the photoreceiver, including noise added by the photodetector and the amplifier, referred to the amplifier input, and c_{sr} is the total offset level due to the background radiation and the photoreceiver electronics referred to the photoreceiver output. If all the noise is included in one term, then

$$y_D = g\{A_T R_v P_0[s(n) * h(n)] + w_T(n) + c_{sr}\}, \qquad (6)$$

where $w_T(n) = A_T R_v b(n) + w(n)$. In Secs. 3 and 4, we analyze the SNR implied by Eq. (6) and the type of photoreceiver used, and we discuss the system basic constraints.

3 System Processing Gain and Signal-to-Noise Ratio

The SNR in a photoreceiver operating in analogue mode can be expressed as[8]

$$\text{SNR} = \frac{P_s}{\sqrt{P_q(P_s + P_b) + \text{NEP}^2 B}}, \qquad (7)$$

where P_s and P_b are, respectively, the optical power of the signal and of the background radiation reaching the photodetector, $P_q = \frac{2FhcB}{\eta\lambda}$, in which F is the excess noise factor of the photodetector, h is the Planck's constant, c is the speed of light, η is the photodetector quantum efficiency, λ is the wavelength, and B is the electrical bandwidth of the photoreceiver. NEP denotes the noise equivalent power of the photoreceiver.

In the absence of background radiation, the optical signal power at which the operation regime of the photoreceiver changes from signal-shot-noise limited SNR to NEP-limited SNR is

$$P_{sk} = \frac{\text{NEP}^2 \eta\lambda}{2Fhc}. \qquad (8)$$

For the used photoreceiver (see Table 1) NEP = $1.2\,10^{-13}$ W Hz$^{1/2}$, and with the values for its APD, $F = 3.45$ and $\eta = 0.78$ at $\lambda = 785$ nm, we find $P_{sk} = 6.45$ nW. For an atmosphere with typical optical coefficients and small- or medium-sized telescopes, the optical power in the photoreceiver is always well below this value if the transmitter is a laser diode. In this case, Eq. (7) can be approximated by

$$\text{SNR} = \frac{P_s}{\text{NEP}\sqrt{B}}. \qquad (9)$$

Note that background radiation would cause an apparent increase in the NEP. Calling NEP$'$ the effective noise equivalent power with background radiation, we have NEP$'^2 = $ NEP$^2 + \frac{2FhcP_b}{\eta\lambda}$. If N pulses are accumulated, the resulting signal-to-noise ratio is SNR$_{ac} = \sqrt{N}$SNR.

Assuming that $y_Q \approx y_D$—where y_Q and y_D are the signals after and before the A/D converter (see Fig. 1) and y_D is given by Eq. (6)—with a good degree of approximation, the processing leading to the recovery of $h(n)$ is accomplished by correlating $y_Q(n)$ with a suitable signal related to the modulating signal $s(n)$. To retrieve the attenuated backscatter through the estimation of $h(n)$, the autocorrelation

Table 1 Parameters of the lidar system prototype.

Parameters	
Laser diode peak power	0.125 W
Wavelength	785 nm
Receiver noise (NEP) (Hamamatsu_C5460SPL5343)	1.2×10^{-13} W Hz$^{-1/2}$
Responsivity of the photodetector	1.02×10^7 V W^{-1}
APD diameter	3 mm
SNR A/D converter	88 dB
A-parameter [Eq. (13)]	6
Number of bits of the A/D converter	16
Telescope diameter (effective area)	0.2 m (0.031 m^2)
Telescope focal ratio	2
Chip duration (adjustable by software)	337 to 675 ns
Bandwidth of optical filter	10 nm
Transmittance of the narrowband optical filter	0.55
Photoreceiver electrical bandwidth	1.5 MHz
Amplifiers based on LMH6624 gain bandwidth	1.5 GHz
Range resolution (adjustable by software)	50 to 100 m
Sequence length	1023 and 2047 bits
Maximum distance (nonambiguous distance)	50 to 200 km
Distance between the beam and telescope axes	0.25 m
Overlap function	Shown in Fig. 7

of the sequence $s(n)$ with that "suitable" signal must be a delta function to avoid a "blurred" profile and the masking of weak returns by strong ones, as would be the case for a cloud behind a weakly scattering aerosol layer.

To modulate the laser transmitted power, pseudorandom M-sequences[9] have the delta-like character of their correlation with the derived sequences

$$s'(n) = 2s(n) - 1, \qquad (10)$$

with $s(n)$ being the original sequence made of ones and zeros.[4–6,9–11] If such a sequence is assumed in Eq. (3), a delta-function will be obtained after the correlation of $s(n)$ with $s'(n)$, with a maximum value of $(N + 1)/2$ when the delay is zero and 0 for the rest of the sequence, N being the sequence length.[4,5,10] The processor block on Fig. 1 will perform the correlation of the A/D converter output with $s'(n)$ for every time shift k to yield

$$z_p(k) = \sum_{n=1}^{N} y_D(n)s'(n + k). \qquad (11)$$

Taking into account Eqs. (5) and (6), one finds

$$z_p(k) \approx \frac{N+1}{2} g A_T R_v P_0 h(k) + g \sum_{n=1}^{N} w_T(n) s'(n+k) + g c_{sr},$$

(12)

where $\sum_{n=1}^{N} s'(n+k) = 1$ has been used.

Clearly, the right side of Eq. (9) above shows that the output of the processor for a shift k contains an estimate of the atmospheric "impulse response," in the term $S_p(k) = \frac{N+1}{2} g A_T R_v P_0 h(k)$, affected by noise contained in the term $N_p(k) = g \sum_{n=1}^{N} w_T(n) s'(n+k)$. The offset term $g c_{sr}$ can be disregarded. However, the effect of a signal offset in practical systems using incomplete sequences in the correlation will be considered in Sec. 5.2. Assuming the samples of $w_T(n)$ independent random variables, the SNR in the estimate of $h(k)$ is, if a number M of the cyclic sequences is processed and the results accumulated,

$$\begin{aligned} \mathrm{SNR}_p(k) &= \frac{\sqrt{M}(N+1) A_T B^{1/2} P_0 h(k)}{2\sqrt{N} \mathrm{NEP}} \\ &\approx \frac{\sqrt{MN} A_T B^{1/2} P_0 h(k)}{2 \mathrm{NEP}}. \end{aligned}$$

(13)

Equation (13) assumes the low-signal approximation for the SNR expressed by Eq. (9).

4 System Basic Constraints

The resulting SNR will be the approximately the same as if a sequence of length MN was used, as other authors have already shown.[4,5,10] The SNR depends on the total integration time rather than on the sequence length. However, using long sequences has an advantage with respect to employing short ones and increasing the accumulation number M because the long sequences increase the unambiguous distance and may have a beneficial effect on the effect of the offset value as discussed in Sec. 5. The unambiguous distance R_{ua} is related to the sequence length through

$$R_{ua} = \frac{c \tau_{\mathrm{bit}} N}{2}.$$

(14)

Therefore, the sequence length must be set to a minimum value $N_{\min} = 2R_{\max}/(c\tau_{\mathrm{bit}})$, where $R_{\max}$ is the maximum range from which nonnegligible returns are expected. Because the range resolution ΔR is given by $\Delta R = c\tau_{\mathrm{bit}}/2$, $N_{\min}$ can be cast as $N_{\min} = R_{\max}/\Delta R$. Values of N above $N_{\min}$ provide a safety margin against unexpectedly high returns (for instance, from clouds) coming from ranges above the nominal one.

Assuming that each bit of the modulating sequence is τ_{bit} seconds long and the laser power in the ON state is P_0, then the energy per ON bit (pulse) is $E_b = P_0 \tau_{\mathrm{bit}}$. Using the parameters of the system described in Sec. 6, with a laser giving a peak power $P_0 = 125$ mW, and $\tau_{\mathrm{bit}} = 655$ ns, the transmitted energy per pulse is 8.19×10^{-8} J.

The most important constraint in this system is the low-energy per transmitted pulse. A transmitter figure of merit, related to the capability of achieving a fixed SNR in a given accumulation time, can be defined as $F_{me} = E\sqrt{\mathrm{PRF}}$, where E is the energy per pulse and PRF is the effective pulse repetition frequency. In our system, the effective pulse repetition frequency is $1/(2\tau_{\mathrm{bit}})$. Taking into account that the energy and the spatial resolution are related by $E_b = P_0 \tau_{\mathrm{bit}} = 2 P_0 \Delta R/c$, where $\Delta R = c\tau_{\mathrm{bit}}/2$ is the spatial resolution, the merit factor can be written as

$$F_{me} = P_0 \sqrt{\frac{\Delta R}{c}}.$$

(15)

This relationship shows that if the laser power is divided by a given value, to maintain the figure of merit (hence a given SNR if everything else remains unchanged) the spatial resolution must be reduced by the square of this value.

This is a handicap in aerosol detection, especially for long-range detection, yet the use of a low peak-power laser is a practical option to increase the life and reduce the cost of the laser component, in addition to increasing eye safety.

5 Effect of Nonlinearity and Offset on the Correlation

In this section, we demonstrate the detrimental effects of receiver nonlinearity in this type of system, which does not seem to have been described in related previous literature.

5.1 Nonlinear Effects

In this type of lidar system, when very low signal is received from the atmosphere, the input y_D of the A/D converter is largely dominated by noise. Even so, if the gain in the receiver amplification parts preceding the A/D converter is too high (or, more unlikely, if the received signal is too strong) there is a risk to driving the amplifiers and converter into the nonlinear region or saturation. The most important problem related to the nonlinearities is the appearance of products between the returned (with different delays) sequences. The results of these products are new sequences that do not meet the correlation criteria of the original sequences.

As shown by Eq. (2), the echo signal consists of a superposition of sequences with different amplitudes and delays. Under saturation or nonlinear behavior of the reception chain, and depending on the sequence delays and amplitudes, the output of the cross-correlation process can show peaks where nothing exists ("ghost" targets), as some authors have reported from employing these pseudorandom sequences in audio applications.[12,13] We have as well observed this phenomenon under specific circumstances in the prototype described in this work.

In the general case, if we have a received signal $y(n)$, the output of the receiver chain before the processing and considering possible nonlinear effects will be

$$y_{nl}(n) = a_0 y(n) + a_1 y^2(n) + a_2 y^3(n) + \ldots,$$

(16)

where $a_0, a_1, a_2 \ldots$ are the coefficients of the linear and nonlinear parts of the response. The received signal $y(n)$ is composed of a sum of replicas of the emitted sequence with the correspondent delay and amplitudes according to Eq. (2). For clarity of the subsequent analysis, we simplify the notation and write $y(n) = b_0 s(n - n_0) + b_1 s(n - n_1) + b_2 s(n - n_2) + \ldots$.
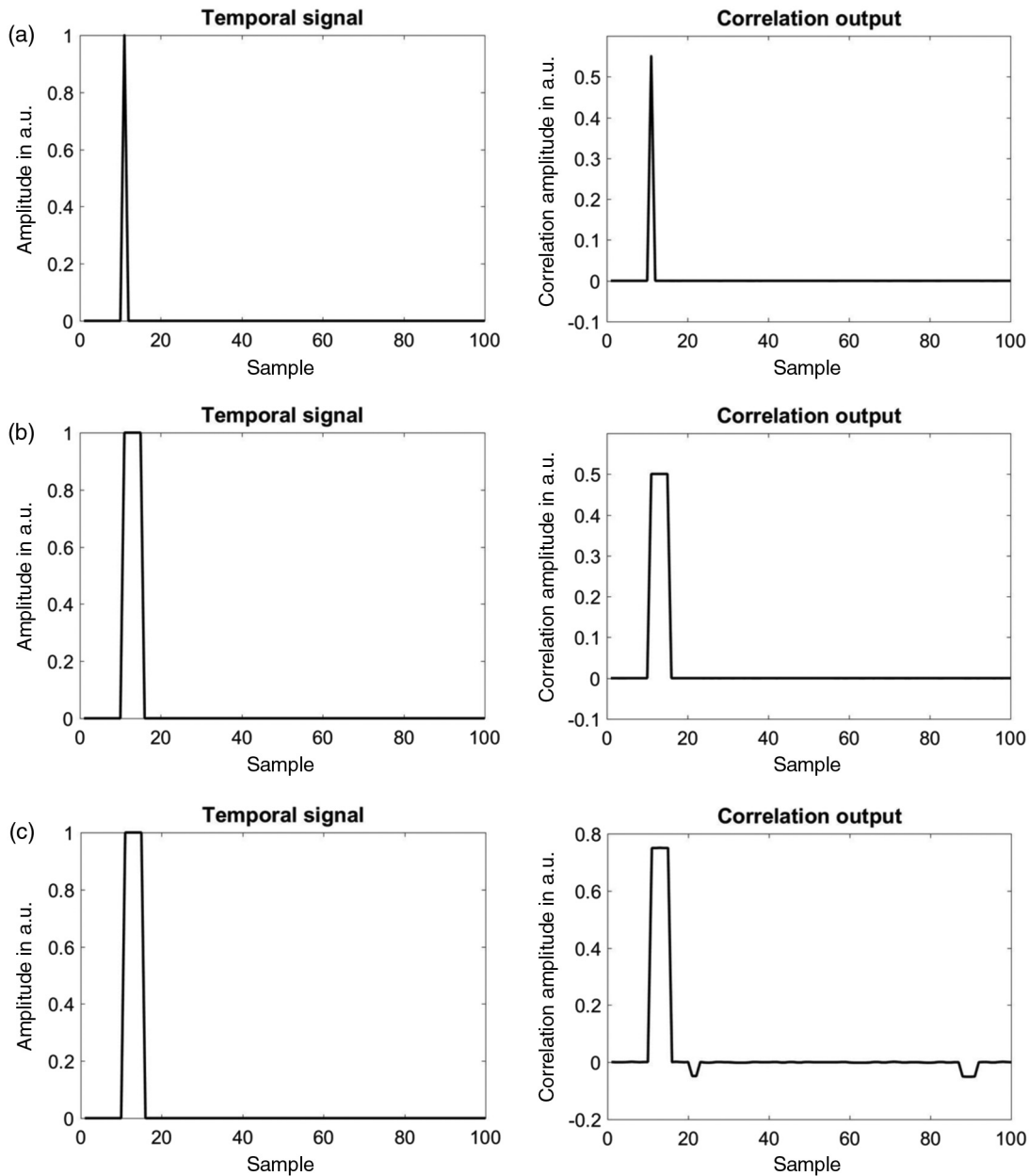
Fig. 2 Simulation of different situations in the received signal and the correlation with the sequence $s'(n)$. An M-sequence of 1023 bits is used. (a) A pure delta function is not sensitive to distortion, (b) a wider function than a delta under linear conditions shows a nondistorted result too, and (c) when this wider signal is correlated after having undergone distortion, an unpredictable number of ghost peaks can appear.

A simple simulation is shown in Fig. 2. Four cases can be found related to the combination of sequences and nonlinearities and its consequences. These are

(1) Only one sequence delayed ($b_k = 0$ for $k > 0$) and linear amplification: the result is correct.

(2) Only one sequence delayed ($b_k = 0$ for $k > 0$) and nonlinear amplification: the result is correct [Fig. 2(a)].

(3) Two or more delays ($b_k > 0$ for some $k > 0$) and linear amplification: the result is correct [Fig. 2(b)].

(4) Two or more delays ($b_k > 0$ for some $k > 0$) and nonlinear amplification: possibility of false (ghost) echoes after the correlation process with $s'(n)$ [Eq. (7)] [Fig. 2(c)].

The first case of the list is trivial and is not represented in the figure. The other cases correspond to the application of Eq. (16) with $a_0 = 1$, $a_1 = 0$, and $a_2 = 0$ (linear case) and with $a_0 = 1$, $a_1 = 0.1$, and $a_2 = 0$ (nonlinear case), to a delta-like temporal received signal (simulating a solid target or very thin target) and with a received signal consisting of five consecutive deltas with same amplitude (simulating a wider layer of clouds and aerosols). The most interesting situation is that of Fig. 2(c). "Ghost" echoes appear when the received signal contains more than an echo and the amplifier is nonlinear (case 4 of the list). These "ghost" echoes appear at any unpredictable position (the analysis is very complex and is out of the scope of this paper).
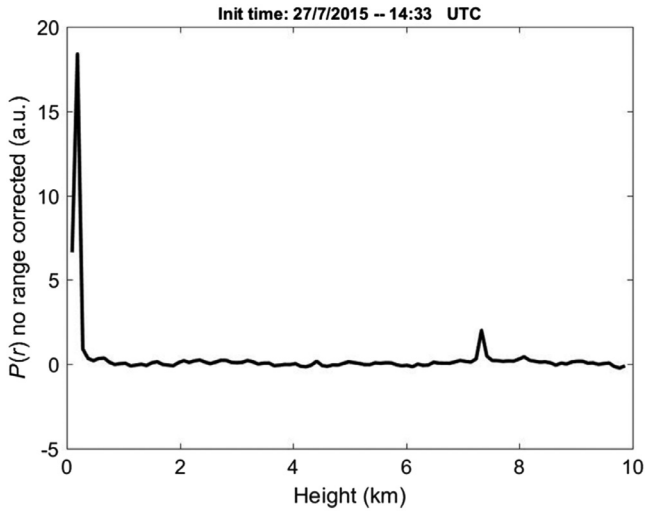
Fig. 3 A real measurement where the effect of the ghost peak is visible. In the 1-D profile the peak is situated 76 samples after the principal peak (equivalent length of 7.6 km).

The simulated effects can be observed under specific circumstances in the test process of the real prototype. Figure 3 shows a real measurement obtained in a test against a solid target close to the lidar to obtain the zero reference (in this case the returned signal is very strong). The first peak is the solid target, and the secondary peak is the ghost peak at the distance of 76 samples. This distance is characteristic of the used length sequence that we have been able to observe under similar situations.

5.2 Effects of Signal Offset

The property of obtaining a delta-like function when the pseudorandom sequence $s(n)$ is correlated with the derived sequence $s'(n)$ (Sec. 3) is true when applying the circular correlation. In the lidar system, it is necessary to capture more samples in the reception process than the transmitted sequence length because of the delay time to measure in the return signal. If N is the sequence length and D is the number of samples waiting for the maximum delay to measure, the correlation (circular) is done between two sequences of length $L = N + D$. The received and sampled signal contains replicas of the transmitted sequence (length N) that delayed the round-trip time to the scattering volume with superimposed noise and offset; D is assumed to be large enough for the last samples of the captured return to contain only noise and offset. The correlation operation in this case will take the form

$$z_p(k) = \sum_{n=1}^{N+D} y_Q(n)s'(n+k). \tag{17}$$
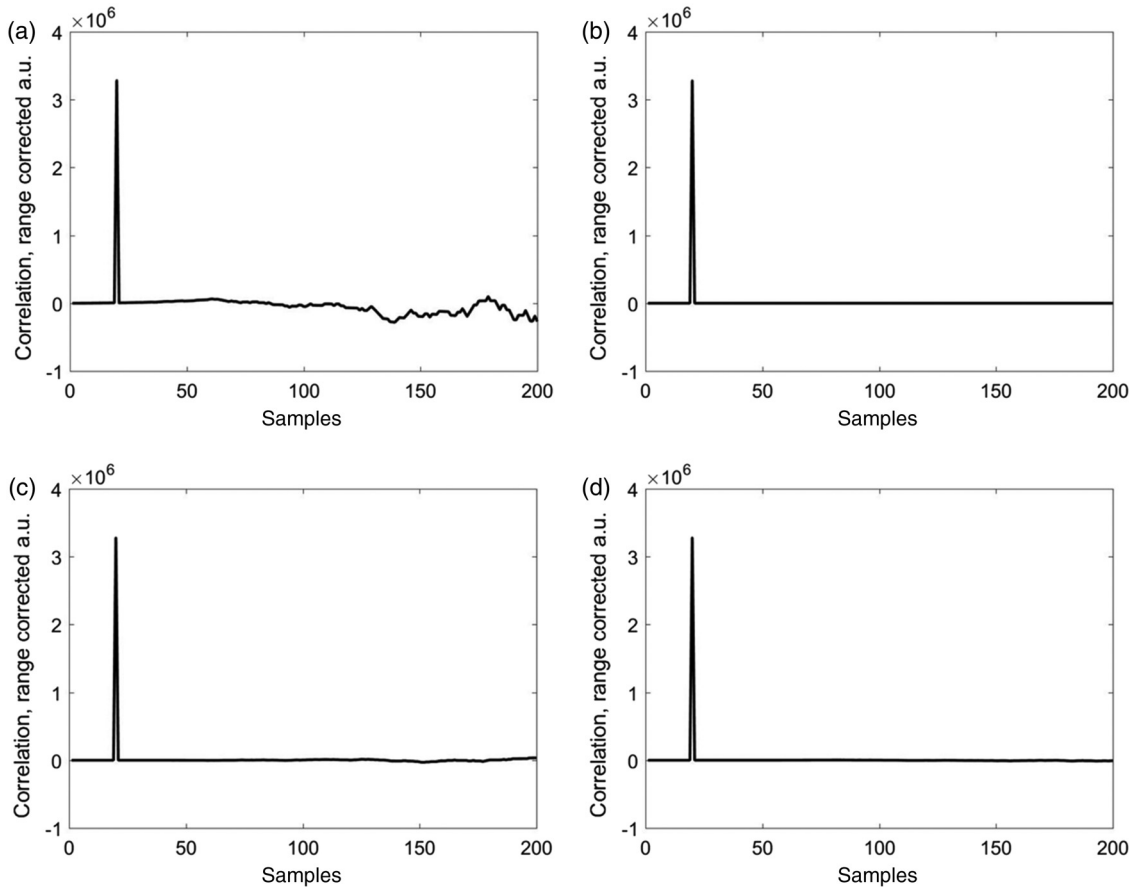
Fig. 4 Simulation of the offset effect on the correlation between incomplete sequences: (a) with $N = 2047$ and $D = 300$, (b) with $2N$ (two complete sequences), (c) and (d) using very long sequences with $N = 16{,}535$ and $D = 300$ bits, and $N = 262{,}143$ and $D = 300$ bits, respectively. A delta-like target is assumed to be at sample number 20 and the offset level has been taken to be equal to the amplitude of the received signal.

The difference between the number of ones and minus ones in different sections of length D of the sequence $s'(n)$ varies, which can give rise to spurious oscillations in $z_p(k)$ in the presence of an offset level (whether originating from the receiver electronics, induced by background radiation, or by both causes) in $y_Q(n)$. This is illustrated in the simulations of Fig. 4, where there is assumed a delta-like target at sample number 50 and an offset level equal to the amplitude of the received signal.

This undesired effect can be avoided, increasing the receiving time to acquire $2N$ samples, i.e., making $D = N$, which ensures that the difference between the numbers of ones and zeros in the interval is constant. This solution has the drawback of being energetically inefficient, as ~50% of the time the system is idle.

Another, more energetically efficient solution to this problem is the use of very long sequences, with N in the order of 10^5 bits, which is feasible with a short processing time with the current DSP state of the art, while keeping D constant. In this way, the effect of the varying number of ones and minus ones in sections of D bits in $s'(n + k)$ in

the presence of a signal offset keeps limited, whereas the signal increases approximately as N [Eq. (9)].

The effects of the proposed solutions in the cross-correlation function can be observed in Fig. 4. The offset effect disappears for $L = 2N$ [Fig. 4(b)] and is greatly reduced for $N \gg D$ [Figs. 4(c) and 4(d)]. The offset effect on a real measurement is shown in Fig. 5.

6 Experimental Prototype and Results

A complete lidar system has been built and tested in a real environment and under real conditions of operation. The core of the lidar system is a DSP and the software to control all the processes. The use of a software-defined lidar allows for changing the operation mode of the system with the same hardware.

Sequence lengths of 1023 and 2047 bits have been considered initially in the experimental prototype, but these can be modified very easily. Even using long sequences of tens
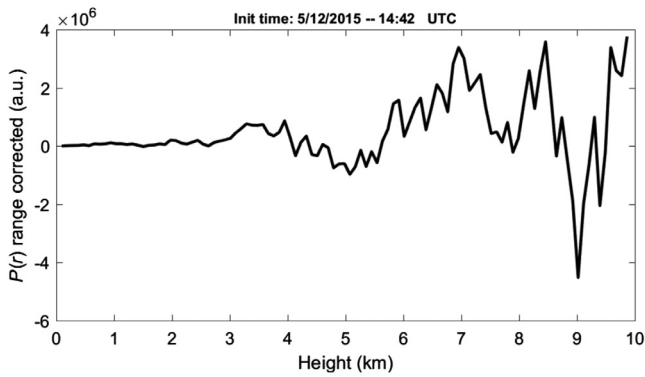

Fig. 5 Real measurement showing the signal offset effect that occurs when a noninteger number of sequences is used in the correlation process ($N = 4096$ bits, $D = 300$ bits).
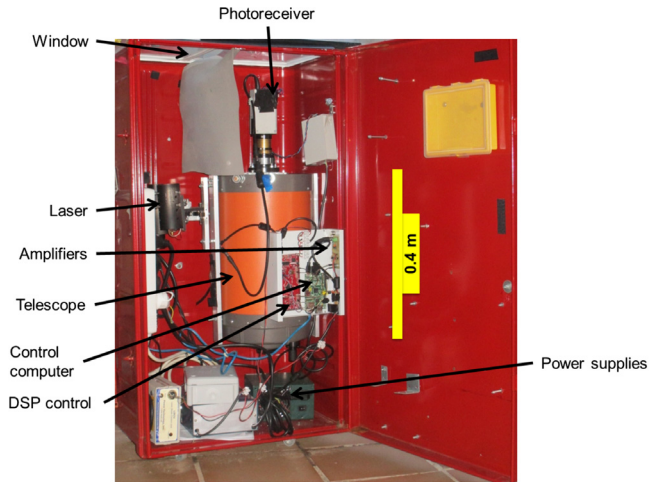

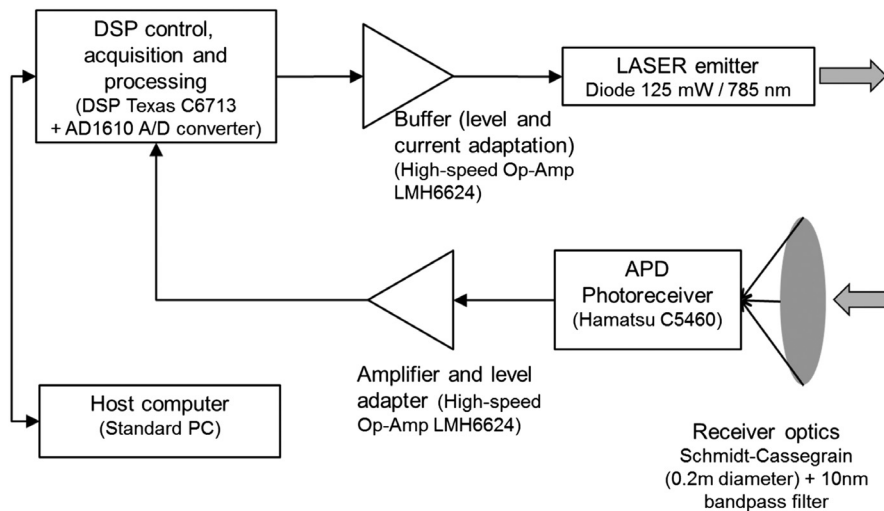**Fig. 7** The lidar prototype mounted in the enclosure.

Fig. 6 Experimental setup layout. A buffer between DSP and laser emitter is necessary to adapt the logical levels of the DSP output to the amplitude necessary to modulate the laser emitter. Both amplifiers in emission and reception are wide bandwidth (1.5 GHz) and ultralow noise op-amp. High bandwidth is necessary to have a fast commutation in the emitted pulses and a low noise amplifier is good in the receiver chain.

or hundreds of thousands of bits, the processing power of the state of the art DSPs makes it possible to neglect the processing time. The time dominating the system is almost exclusively the integration tim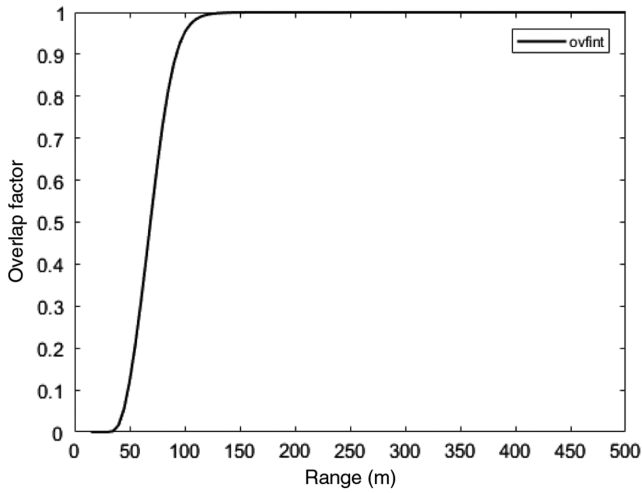e, except if very short sequences are used, when the processing time dominates. The lidar system parameters are listed in Table 1. The layout of the experimental setup is detailed in Fig. 6.

The equipment, which is operated day and night in an autonomous mode, is shown in Fig. 7. Note that the scale reference in the figure gives an idea of its compactness. The photodetector is in the primary focus of a Schmidt–Cassegrain telescope with the secondary mirror removed to simplify the alignment of the laser inside the field of view (wider field of view), resulting in an $f/2$ telescope. Figure 8 shows the calculated overlap function of the system.

Figure 9 shows different examples of cloud detection. Figure 9(a) shows a medium-high cloud evolving between 3- and 5-km altitude, and at the end of the measurement interval a high cloud at around 8 km appears. Figures 9(b) and 9(c) show high altitude clouds between 7 and 8 km. Figure 9(c) is the 1-D profile resulting from the integration of the profiles in the measurement interval of Fig. 9(b). In Fig. 9(d), the detection of a low cloud and rain is noticed. The measurements of Fig. 9 have been obtained using M-derived A-sequences,[11] which have properties close to those of M-sequences, the circular correlation of an A-sequence with a shifted one yielding a peak for zero shift and a small ripple of constant amplitude for other shifts.
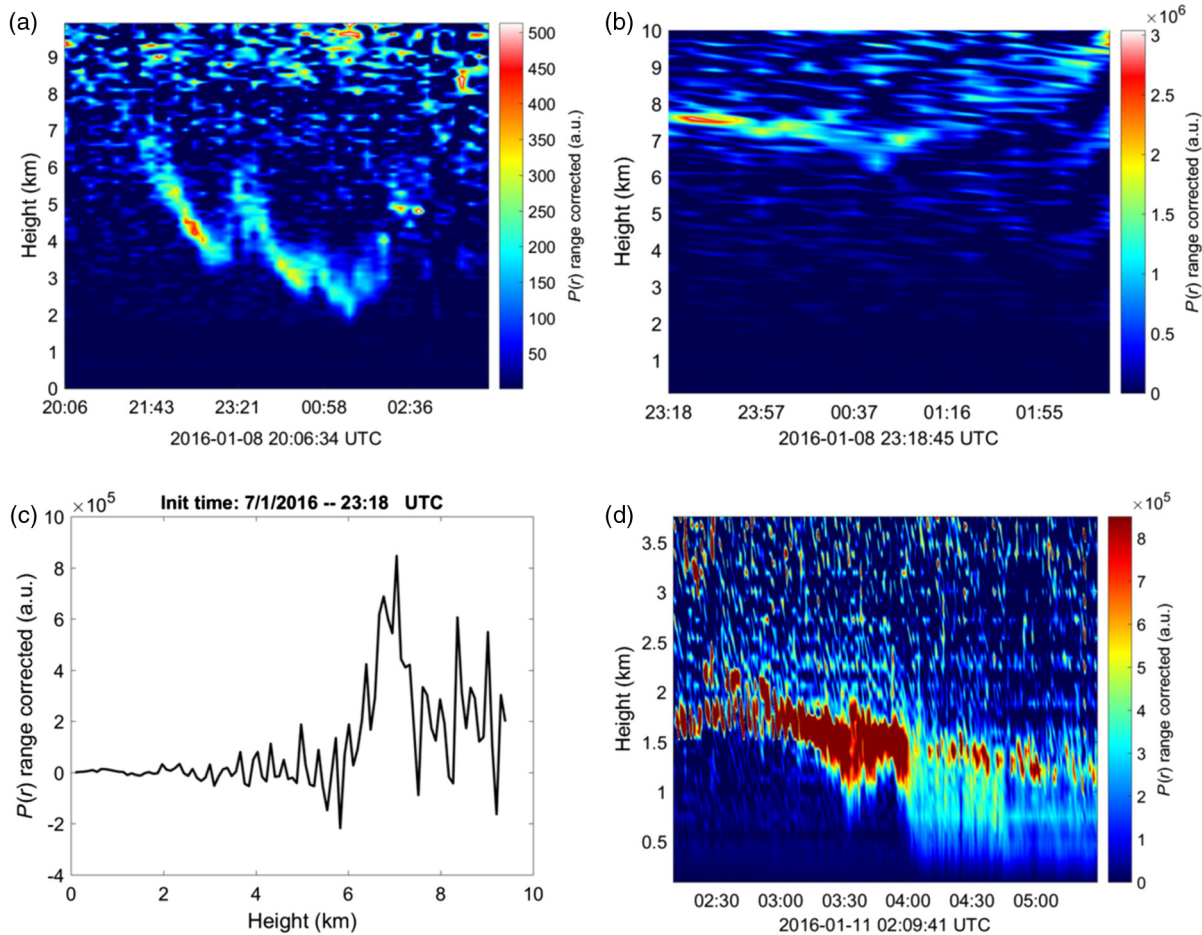

Fig. 8 Calculated overlap function of the experimental lidar system.

Fig. 9 Cloud detection with the constructed prototype. (a) Medium height clouds between 3 and 5 to 6 km, and at 8 km at the end of measurement period, (b) high clouds at 7 to 8 km, (c) profile 1-D resulting from the integration in the time interval of panel (b), and (d) low clouds and rain detected at the end of the night in the presence of a low cloud layer. Temporal resolution: 4 min for (a) and (b), 30 s for (d). Spatial resolution is 100 m in all the cases. Sequence: $A1$ type of 2047 bits.[11]
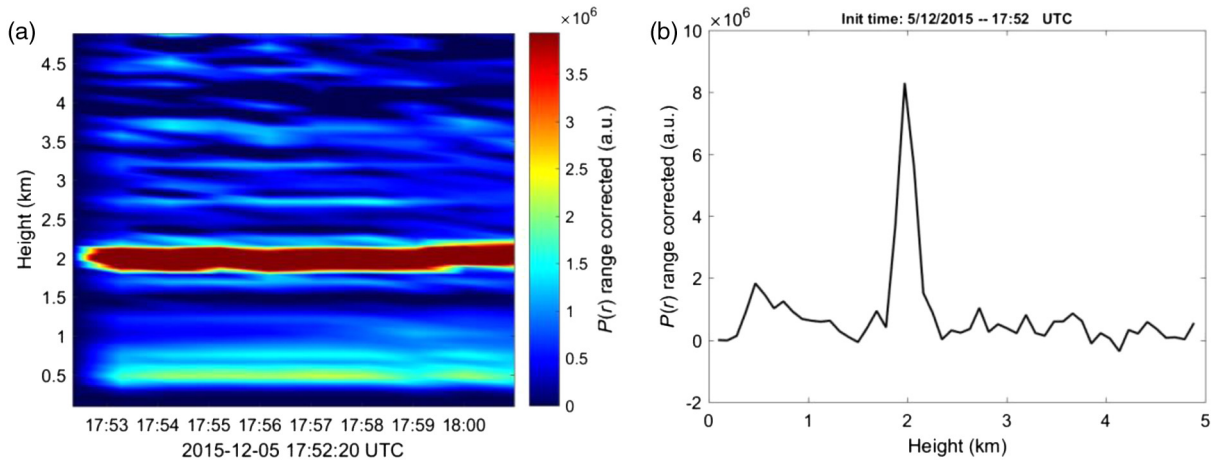
Fig. 10 (a) Range-corrected time-height graph showing a cloud at about 2 km and aerosol below it; time resolution: 17 s, space resolution 50 m. (b) Accumulation of all the profiles in panel (a) showing the cloud and the aerosol signatures. Sequence: *A*2 type of 4091 bits.[11]
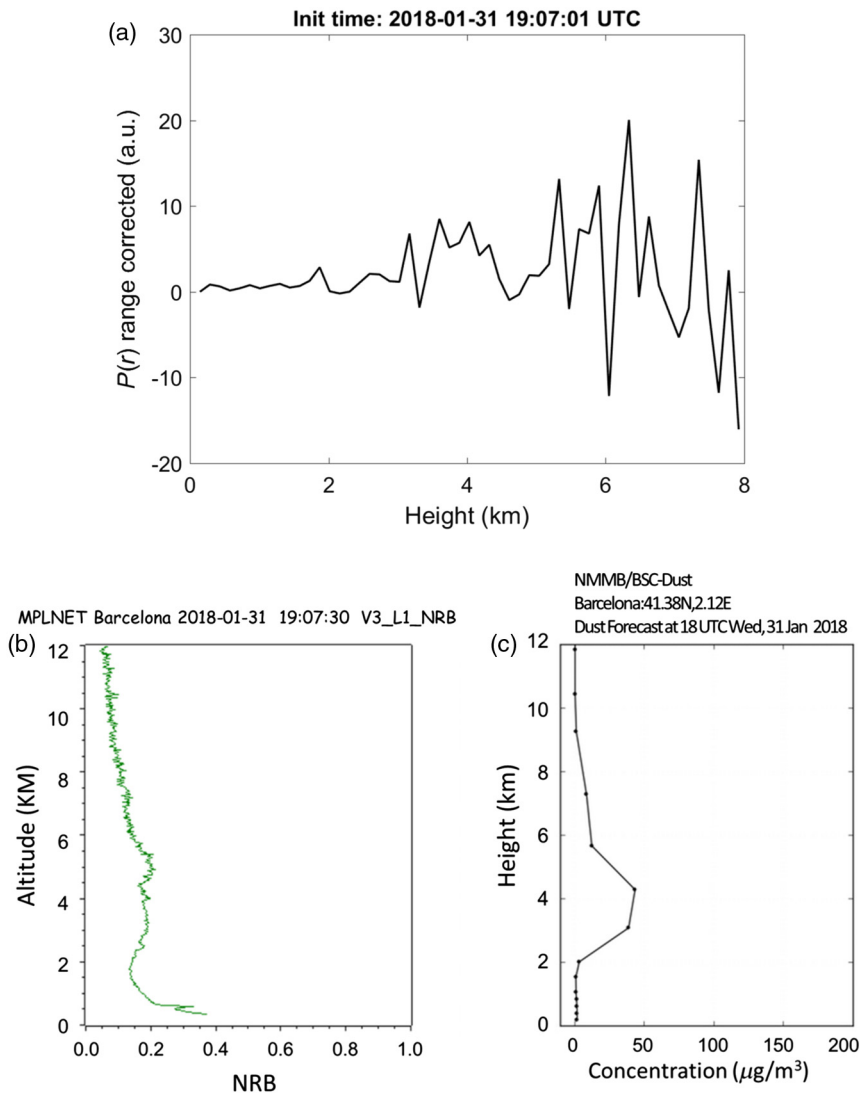
Fig. 11 (a) Range-corrected time-height graph showing a Saharan dust layer above Terrassa, where the prototype described in this paper was being operated. (b) Normalized relative backscatter (NRB, essentially range- and overlap-corrected signal) measured by the MPL lidar operating at Universitat Politècnica de Catalunya (UPC) Barcelona,[14] 20 km away from Terrassa. (c) The predicted dust concentration profile at Barcelona from the Barcelona Supercomputing Center (BSC) (image from the NMMB/BSC-Dust model, operated by the Barcelona Supercomputing Center).[15]

Although detection of clouds with pseudorandom power-modulation lidar has been presented previously,[5,10] to our knowledge, this is the first time that detection of clouds as high as 8 km is reported for a system employing a low-power transmitter in the infrared and an APD in the receiver.

Figure 10 corresponds to a 20-min measurement showing a cloud deck with the base slightly below 2 km and aerosol below it. Figure 10(a) is the time-height representation with a 1-min temporal resolution and 50-m spatial resolution. Figure 10(b) is the 1-D representation corresponding to the accumulation of all the profiles in the 20-min interval. Figure 10 has also been obtained using an A-sequence.

Figure 11 shows measurement results during a Saharan dust outbreak in Barcelona. Figure 11(a) corresponds to the integration of 30 consecutive measurements of 1 min each obtained with the lidar described in this paper, operating in the city of Terrassa, 20 km to the Northwest from Barcelona, at 19 h UTC on the January 31, 2018. The layer is visible at 3 to 4 km of altitude through the "bump" in the range-corrected signal profile. Figure 11(b) shows the measurement obtained with the micropulse lidar (MPL) operating at the UPC Campus in Barcelona, at approximately the same moment with a 30-s averaging time, where a similar feature is found in the normalized relative backscatter profile (essentially the range- and overlap-corrected signal); in this case, an increase in the signal at very low altitude is due to boundary-layer aerosols revealed by the overlap correction (it should be noted that the MPL system has a figure of merit as defined in Sec. 4 four orders of magnitude higher than that of our system and that it uses a photon-counting receiver). Figure 11(c) is the dust forecast from the BSC (Barcelona Supercomputing Center) for approximately the measurement time (18-h UTC).

7 Conclusions

We have shown that a compact, all-semiconductor PRN lidar working with limited laser peak power and using an APD-based receiver in linear mode, with a low overall power requirement for the whole system (<10 W) can offer an alternative to present ceilometer systems. Detection of clouds as high as 8 km, as well as that of low-altitude aerosols, has been demonstrated, with the latter needing longer integration times. The use of very long sequences while maintaining low values of correlation time using DSPs allows for increasing the nonambiguous range and suppressing artifacts produced by offsets at the input of the correlator. Some cautions have to be taken into account in the system design. One of the most important is to avoid saturation and distortion in the photoreceiver system because of their effects on the correlation of the received signal with the sequence used to retrieve the spatial information, which can result in the appearance of ghost targets. The length of the acquired signal is also of concern for avoiding artifacts in the presence of (unavoidable) offsets at the photoreceiver output.

Moreover, the design and construction of this system needs to achieve a good decoupling between the emitter and receiver subsystems because they are operating simultaneously with a huge difference in the signal levels.

The use of a DSP simplifies the implementation of this system in that the behavior is software defined. The DSP can carry out the whole process such as sending and

receiving, the signal correlation, and the implementation of any inversion algorithm if it is necessary.

New steps are being taken in the direction of using a new family of DSP-microcontrollers in one chip to reduce the size, power consumption, and circuit complexity to obtain a more compact lidar and system.

References

1. C. Muenkel, U. Leiterer, and H.-D. Dier, "Affordable lidar for atmospheric aerosol and cloud studies," *Proc. SPIE* **4484**, 198–206 (2002).
2. J. Lindholm, "An analysis of the pseudo-randomness properties of subsequences of long m-sequences," *IEEE Trans. Inf. Theory* **14**(4), 569–576 (1968).
3. M. Goresky and A. Klapper, "Pseudonoise sequences based on algebraic feedback shift registers," *IEEE Trans. Inf. Theory* **52**(4), 1649–1662 (2006).
4. N. Takeuchi et al., "Diode-laser random-modulation cw lidar," *Appl. Opt.* **25**(1), 63–67 (1986).
5. N. Takeuchi et al., "Random modulation cw lidar," *Appl. Opt.* **22**(9), 1382–1386 (1983).
6. P. Vujkovic-Cvijin et al., "Diode-laser-based lidars: the next generation," *Proc. SPIE* **3758**, 142–151 (1999).
7. R. T. H. Collis and P. B. Russell, in *Laser Monitoring of the Atmosphere*, Lidar measurement of particles and gases by elastic backscattering and differential absorption, E. D. Hinkley, Ed., p. 76, Springer-Verlag, Berlin (1976).
8. R. R. Agishev et al., "Application of the method of decomposition of lidar signal-to-noise ratio to the assessment of laser instruments for gaseous pollution detection," *Appl. Phys. B* **79**(2), 255–264 (2004).
9. F. J. MacWilliams and N. J. A. Sloane, "Pseudo-random sequences and arrays," *Proc. IEEE* **64**(12), 1715–1729 (1976).
10. R. Matthey and V. Mitev, "Pseudo-random noise-continuous-wave laser radar for surface and cloud measurements," *Opt. Lasers Eng.* **43**(3–5), 557–571 (2005).
11. C. Nagasawa et al., "Random modulation cw lidar using new random sequence," *Appl. Opt.* **29**(10), 1466–1470 (1990).
12. J. Vanderkooy, "Aspects of MLS measuring systems," *J. Audio Eng. Soc.* **42**(4), 219–231 (1994).
13. G.-B. Stan, J.-J. Embrechts, and D. Archambeau, "Comparison of different impulse response measurement techniques," *J. Audio Eng. Soc.* **50**(4), 249–262 (2002).
14. https://mplnet.gsfc.nasa.gov/data?v=V3&s=Barcelona&t=20180131 (13 April 2018).
15. http://www.bsc.es/ess/bsc-dust-daily-forecast/ (13 April 2018).

Antoni Ardanuy is a free-lance electrical engineer pursuing his PhD degree at the Department of Signal Theory and Communication of Universitat Politècnica de Catalunya (UPC-Barcelonatech).

Adolfo Comerón is a professor with the Department of Signal Theory and Communications at Universitat Politècnica de Catalunya (UPC-BarcelonaTech), Barcelona, Spain. His research activities have included the study of nonlinear devices at IR wavelengths and the development of microwave and millimeter-wave receivers for satellite communication systems. They currently focus on lidar remote sensing and free-space optical communications. He is member of SPIE and IEEE.